NEATH IV: an early onset of complex organic chemistry in molecular clouds

F. D. Priestley,[1]★ P. C. Clark [1], S. E. Ragan [1], S. Scibelli [2]†, M. T. Cusack [1], S. C. O. Glover [3], O. Fehér,[1] L. R. Prole[4] and R. S. Klessen [3,5,6,7]

[1]*School of Physics and Astronomy, Cardiff University, Queen's Buildings, The Parade, Cardiff CF24 3AA, UK*
[2]*National Radio Astronomy Observatory, 520 Edgemont Road, Charlottesville, VA 22903-2475, USA*
[3]*Zentrum für Astronomie, Institut für Theoretische Astrophysik, Universität Heidelberg, Albert-Ueberle-Straße 2, D-69120 Heidelberg, Germany*
[4]*Centre for Astrophysics and Space Science Maynooth, Department of Theoretical Physics, Maynooth University, W23 F2H6 Maynooth, Ireland*
[5]*Interdisziplinäres Zentrum für Wissenschaftliches Rechnen, Universität Heidelberg, Im Neuenheimer Feld 205, D-69120 Heidelberg, Germany*
[6]*Harvard-Smithsonian Center for Astrophysics, 60 Garden Street, Cambridge, MA 02138, USA*
[7]*Elizabeth S. and Richard M. Cashin Fellow at the Radcliffe Institute for Advanced Studies at Harvard University, 10 Garden Street, Cambridge, MA 02138, USA*

ABSTRACT

Complex organic molecules (COMs) are widely detected in protostellar and protoplanetary systems, where they are thought to have been inherited in large part from earlier evolutionary phases. The chemistry of COMs in these earlier phases, namely starless and prestellar cores, remains poorly understood, as models often struggle to reproduce the observed gas-phase abundances of these species. We simulate the formation of a molecular cloud, and the cores within it, out of the diffuse interstellar medium, and follow the chemical evolution of the cloud material starting from purely atomic initial conditions. We find that the formation of both gas- and ice-phase COMs precedes the formation of cores as distinct objects, beginning at gas densities of a few $10^3 \, \mathrm{cm}^{-3}$. Much of this COM-enriched material remains at these relatively modest densities for several Myr, which may provide a reservoir for accretion onto planet-forming discs in later evolutionary stages. We suggest that models of core and disc chemistry should not ignore the complex dynamical evolution which precedes these structures, even when studying supposedly late-forming molecules such as CH_3OH and CH_3CN.

Key words: astrochemistry – stars: formation – ISM: clouds – ISM: molecules.

1 INTRODUCTION

Complex organic molecules (COMs), in an astrochemical context, are those made up of six or more atoms, including at least one of carbon (Herbst & van Dishoeck 2009). They are widely detected towards protostellar and protoplanetary systems via both emission from gas-phase COMs (e.g. Jørgensen et al. 2016; Walsh et al. 2016; Ceccarelli et al. 2017) and, increasingly, mid-infrared absorption features caused by COMs in icy mantles around dust grains (McClure et al. 2023; Nazari et al. 2024; Rocha et al. 2024). In either form, they are likely to be incorporated into planets forming within these systems (Öberg & Bergin 2021), and represent a potential starting point for the formation of amino acids and other molecules with important biological roles on Earth. There has thus been significant interest in the potential connection between interstellar COMs and the origins of life (e.g. Jiménez-Serra et al. 2020).

The presence of COMs in protostellar cores is generally understood to result from their formation in ice mantles during the preceeding prestellar phase, which are subsequently evaporated into the gas phase by protostellar heating (Viti et al. 2004; Garrod & Herbst 2006). This picture struggles to explain the widespread detection of gas-phase COMs in starless and prestellar cores (Jiménez-Serra et al. 2016; Scibelli & Shirley 2020; Ambrose, Shirley & Scibelli 2021; Jiménez-Serra et al. 2021; Mininni et al. 2021; Scibelli et al. 2021; Punanova et al. 2022; Megías et al. 2023), which have no internal heating source. Detections of COMs in diffuse and translucent clouds (e.g. Liszt et al. 2018) raise similar problems, as the densities should be to low to allow their formation on grain surfaces. Suggested resolutions to these issues include enhanced reactive desorption efficiencies (Vasyunin et al. 2017; Riedel et al. 2023), external irradiation (Spezzano et al. 2022; Jensen et al. 2023), and non-diffusive surface chemistry (Jin & Garrod 2020; Garrod et al. 2022), but at present no consensus has been reached on the correct explanation. As the chemical makeup of protostellar systems is in large part inherited from the prestellar phase (Booth et al. 2021; Jensen et al. 2021b), this severely limits our ability to understand the delivery of COMs to planets forming within these systems.

The vast majority of modelling efforts regarding COM chemistry in cores neglect the physical evolution of the system entirely, assuming the density (or density profile) remains static for the entire

★ E-mail: priestleyf@cardiff.ac.uk
† Jansky Fellow of the National Radio Astronomy Observatory

~ Myr duration of the chemical simulation. Models also typically assume the chemical initial conditions are atomic (with the exception of H_2), or representative of a prior 'diffuse cloud' evolutionary phase. However, cores form in the dynamic environments of molecular clouds, which can have a significant impact on their chemistry when compared to static models (Jensen et al. 2021a; Clément et al. 2023; Priestley et al. 2023a). In particular, molecular cloud material can undergo multiple transient enhancements to relatively high densities ($> 10^3$ cm^{-3}) before being incorporated into a gravitationally bound core (Priestley et al. 2023b), so the assumption of chemical initial conditions corresponding to atomic or diffuse molecular gas is unlikely to be applicable to real objects.

In this paper, we investigate the origins of COMs starting from the cold neutral phase of the interstellar medium (ISM), where even hydrogen is in atomic form. Using hydrodynamical simulations coupled to a time-dependent gas-grain chemical network (Priestley et al. 2023a), we can simultaneously and self-consistently follow both the formation of cores from the diffuse ISM, and the build-up of chemical complexity from pristine initial conditions. We find that the formation of significant quantities of COMs occurs before the formation of the cores themselves as distinct objects. The molecular composition of protostellar systems may be inherited not just from the prestellar phase but from the parent molecular cloud itself, making it essential to consider the full evolutionary history of a system when modelling its chemistry.

2 METHOD

We perform magnetohydrodynamical simulations using the AREPO moving-mesh code (Springel 2010; Pakmor, Bauer & Springel 2011), with the addition of a comprehensive suite of physical processes to model the thermodynamical evolution of the gas and dust (Glover & Mac Low 2007; Glover & Clark 2012; Clark et al. 2012b). This includes a simplified chemical network for the formation of H_2 and CO, based on Gong, Ostriker & Wolfire (2017) with some changes as described in Hunter et al. (2023), and a self-consistent treatment of shielding from the background ultraviolet (UV) radiation field (Clark, Glover & Klessen 2012a). Sink particles, representing newly formed stars or stellar systems (Bate, Bonnell & Price 1995), are introduced with a threshold density of 2×10^{-16} g cm^{-3} and a formation radius of 9×10^{-4} pc, following the criteria for creation from Tress et al. (2020).

Our simulation consists of two spherical, uniform-density 10^4 M$_\odot$ clouds of radius 19 pc, for an initial number density of hydrogen nuclei $n_H = 10$ cm^{-3}, with their centres separated by 38 pc so the clouds are initially just touching. The clouds are given a turbulent velocity field with velocity dispersion 0.95 km s^{-1}, bulk motions of 7 km s^{-1} toward each other, and a magnetic field of 3 μG along the collision axis. Initial gas and dust temperatures are set to 300 and 15 K respectively. The background UV radiation field is set to 1.7 times the Habing (1968) value, the cosmic ray ionization rate to 10^{-16} s^{-1} per H atom (consistent with estimates for the diffuse ISM and molecular clouds; Indriolo et al. 2015; Sabatini, Bovino & Redaelli 2023), the dust-to-gas ratio to 0.01, and the carbon and oxygen abundances to the values in Table 1, taken from Sembach et al. (2000). The 'metal' abundance, representing heavier elements such as silicon, is set to 10^{-7}. The simulation is run for 5.53 Myr, by which point 102 M$_\odot$ of material (0.5 per cent of the intiial mass) has been converted into sink particles.

We use Monte Carlo tracer particles (Genel et al. 2013) to follow the evolution of individual parcels of gas through the simulation, recording the properties of their parent cells at intervals of 44 kyr.

Table 1. Elemental abundances used in the chemical modelling.

Element	Abundance	Element	Abundance
C	1.4×10^{-4}	S	1.2×10^{-5}
N	7.6×10^{-5}	Si	1.5×10^{-7}
O	3.2×10^{-4}	Mg	1.4×10^{-7}

We select 10^5 of these particles with final densities in the range $10^2 - 10^6$ cm^{-3}, and use their evolutionary histories to calculate the chemical composition with the NEATH framework[1] (Non-Equilibrium Abundances Treated Holistically; Priestley et al. 2023a). This involves using the time-dependent gas-grain code UCLCHEM (Holdship et al. 2017) to evolve the UMIST12 (McElroy et al. 2013) reaction network, with some modifications to ensure the results are consistent with the internal AREPO abundances of H_2 and CO. Adopted elemental abundances are listed in Table 1; these are also taken from Sembach et al. (2000), with silicon and magnesium reduced by a factor of 100 to represent their incorporation into refractory dust grains in the denser ISM (Jenkins 2009).

In addition to the gas-phase reactions, UCLCHEM also models grain surface chemistry by tracking the freeze-out of molecules onto grain surfaces and their subsequent desorption back into the gas phase. Depletion rates are calculated following Rawlings et al. (1992), and desorption via H_2 formation, cosmic ray impacts, and the UV field (both background and cosmic ray-generated) is modelled using the approach of Roberts et al. (2007). We assume desorption efficiencies of 0.01 molecule per H_2 formation, 10^5 per cosmic ray impact, and 0.1 per UV photon, as recommended in Roberts et al. (2007). The reaction network we use here does not explicitly include reactions between ice mantle species, but allows for some fraction of depleted molecules to be hydrogenated instantaneously upon incorporation into the ice phase.

In this paper, we focus on two of the simplest COMs: methanol (CH_3OH) and methyl cyanide (CH_3CN). As well as representing the broader O- and N-bearing families of COMs, the two molecules have distinct formation pathways. In our chemical network, methanol is formed by the hydrogenation of CO on grain surfaces, which we assume happens with an efficiency of $f_{CH_3OH} = 0.1$ – two separate CO freeze-out reactions are included in the network, the products being either CO or CH_3OH ice, with branching ratios (0.9 and 0.1, respectively) modifying the base rate for CO depletion. Ice-phase CH_3OH participates in no reactions other than desorption processes, while gas-phase CH_3OH undergoes two-body reactions, photodissociation and freeze-out in an identical manner to other species in the network. We find that this value of f_{CH_3OH} produces a good agreement with observed methanol abundances in cores, but our main conclusions hold regardless of the precise value chosen (see Fig. 7). The impact of the underlying assumptions of this model, such as instantaneous hydrogenation, are discussed in Section 4.1. Methyl cyanide is only formed via gas-phase reactions, primarily by the reaction between CH_3^+ and HCN to form CH_3CNH^+ followed by recombination with free electrons. We adopt the dissociative re-combination reaction rate recommended by Giani et al. (2023) rather than the UMIST12 value; we discuss this choice in Appendix A.

3 RESULTS

Fig. 1 shows column density maps of total hydrogen nuclei (N_H), and of gas- and ice-phase CO, CH_3OH, and CH_3CN after 5.53 Myr,

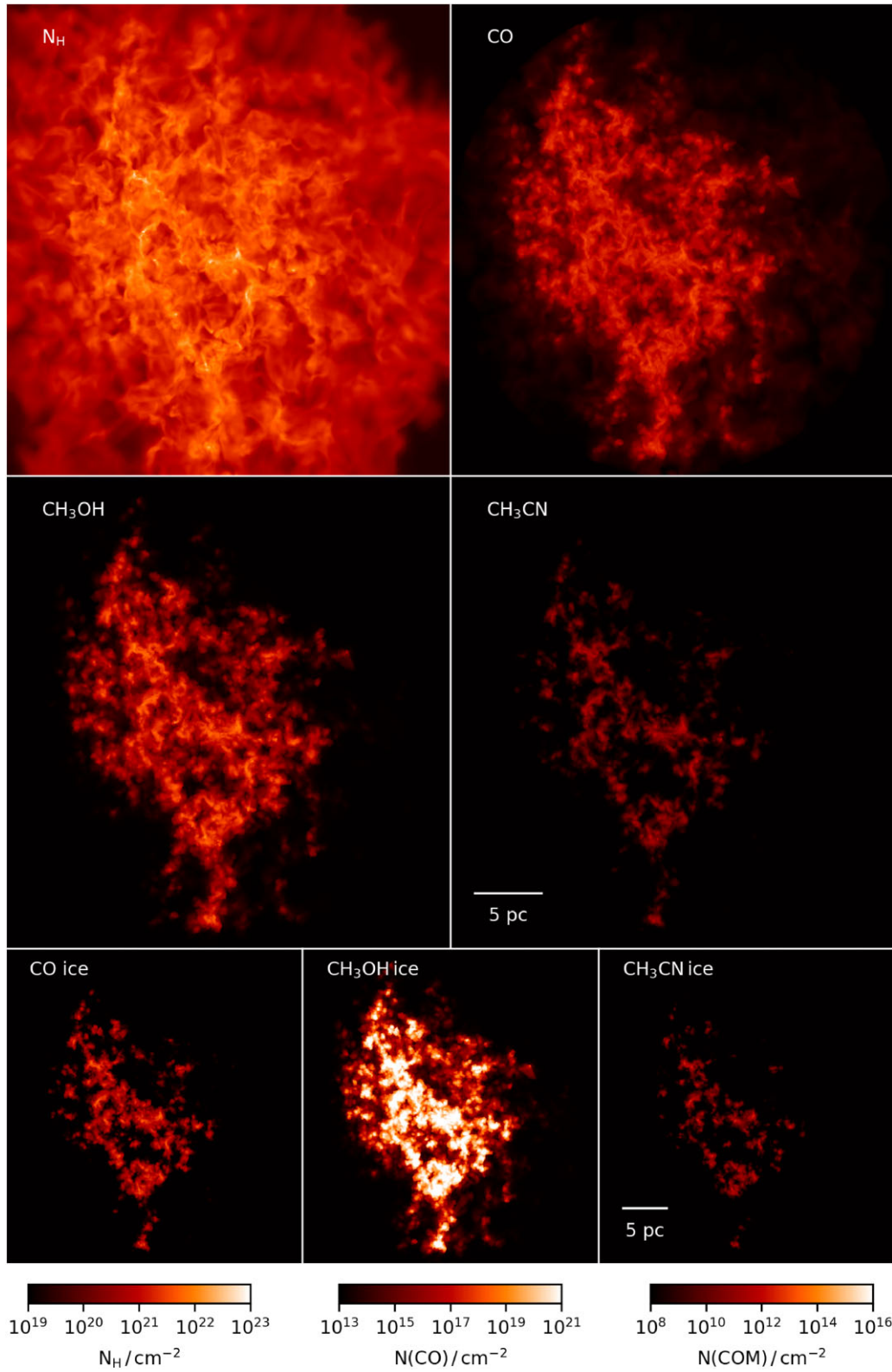[1] https://fpriestley.github.io/neath/

Figure 1. Column density maps at 5.53 Myr of total hydrogen nuclei, and of CO, CH$_3$OH, and CH$_3$CN in gas and ice phases. The colour bars correspond to total hydrogen nuclei (left) and the gas- and ice-phase columns of CO (centre) and of both COM species (right).

by which point the initially atomic clouds have formed a substantial mass of denser molecular material at the collision interface. Much of the diffuse structure seen in the total column map is not visible in any molecular tracer, with CO being restricted to the denser, better-

shielded regions of the cloud. CH$_3$OH and CH$_3$CN are even more limited in terms of the fraction of cloud area with significant column densities. However, they are not entirely restricted to the peaks in the column density distribution; substantial gas-phase columns of both
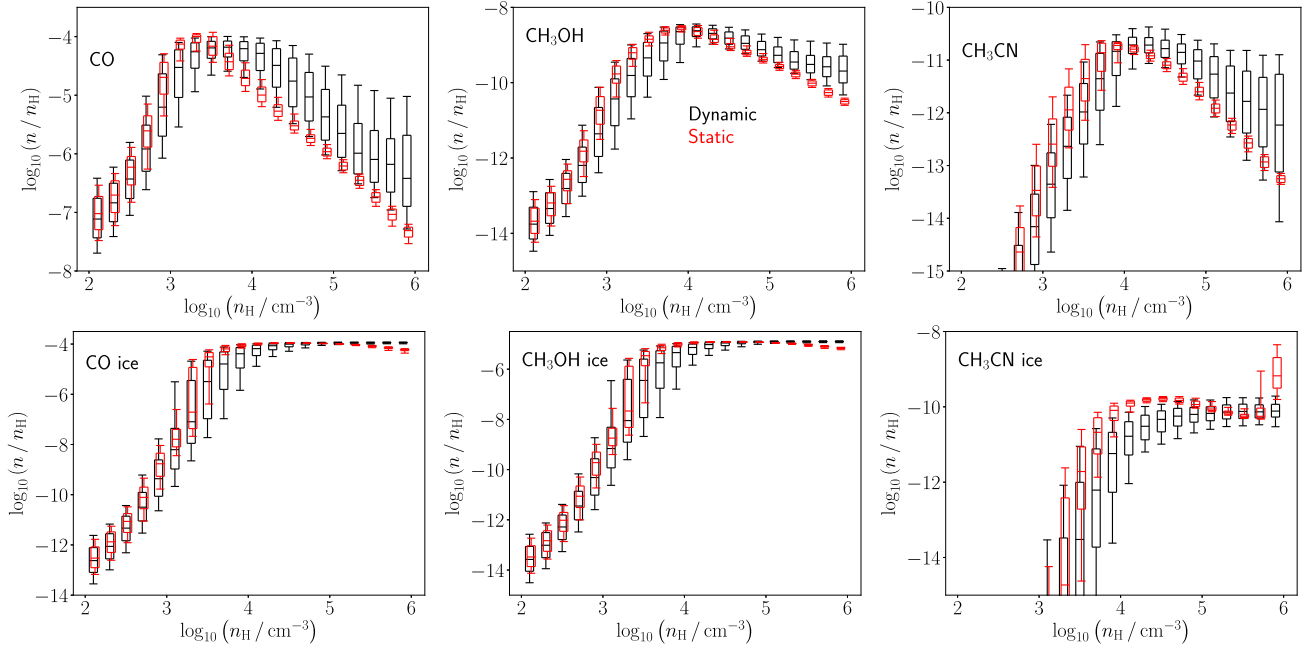
Figure 2. Abundances of gas-phase (top row) and ice-phase (bottom row) CO (left), CH$_3$OH (centre), and CH$_3$CN (right) as a function of gas density at 5.53 Myr, for chemical models utilizing the full tracer histories (black) or holding physical properties constant at their final values (red). Boxes show median values and 25th/75th percentiles, whiskers the 10th/90th percentiles.

COMs exist along moderate-density sightlines through the cloud. This is also true for the ice-phase column densities which are again extended beyond the 0.1 pc-scale core structures, although to a lesser extent for CH$_3$CN ice, which requires particularly high densities to both form in the gas-phase and then deplete onto grain surfaces.

Fig. 2 shows the distribution of CO, CH$_3$OH, and CH$_3$CN abundances in both gas and ice phases as a function of volume density. In all cases, abundances rise sharply to a peak value at densities between 10^{3-4} cm^{-3}, beyond which point gas-phase abundances begin to decline due to freeze-out, while ice-phase abundances remain relatively constant. This decline is less pronounced for CH$_3$OH, where the depletion of the gas-phase molecule is partially balanced by its formation in the mantle via CO depletion and the subsequent desorption of the CH$_3$OH ice.

We also show results for when the physical evolution of the system is ignored: tracer evolutionary histories are modified so that the density, temperature, and shielding columns are equal to their final values for the entire 5.53 Myr duration of the simulation, and the chemical model rerun on these non-evolving histories from the same (atomic) initial conditions as the dynamic model. The approach of evolving the chemistry with fixed physical properties is common in models of COM formation in cores (Vasyunin et al. 2017; Riedel et al. 2023). The two approaches produce broadly consistent results up to densities of $\sim 10^4$ cm^{-3}, as the chemical time-scales are comparable to or shorter than the dynamical time-scales at these densities. The abundances in the dynamic model are therefore quite close to their equilibrium values for densities below 10^4 cm^{-3} (Holdship & Viti 2022; Priestley et al. 2023a; Rawlings, Keto & Caselli 2024), making the use of static chemical models justified in this regime.

At higher densities, however, the static approach significantly underestimates the gas-phase abundances of all species due to allowing an unrealistic degree of freeze-out; the actual amount of time spent at these densities is a tiny fraction of the $\sim$ Myr time-scales over which

static chemical models are typically evolved (Priestley et al. 2023a). CH$_3$OH, with its ice-phase formation pathway, is less affected than CO and CH$_3$CN, as the excess depletion is partially balanced by excess formation via CO freeze-out, but its gas-phase abundance in the static model can still be an order of magnitude lower than the correct value.

In static chemical models of cores, most of the COM content exists in the central, well-shielded regions, where densities are significantly higher than 10^4 cm^{-3} (Vasyunin et al. 2017; Riedel et al. 2023). These models are therefore likely to systematically underestimate the gas-phase abundances of COMs, compared to models with a more realistic treatment of core formation and evolution. Molecular column densities, integrated through the entire cloud, do not vary by more than a factor of $2 - 3$ between static and dynamic models, because the fraction of mass above 10^4 cm^{-3} along the line of sight is rarely high enough for the large abundance differences in this regime to become apparent. However, changing the abundances in this high-density material may have a significant impact on predictions for molecular line emission (e.g. Yin, Priestley & Wurster 2021), particularly for transitions with high critical densities. Chemical models utilizing full evolutionary histories should be preferred when applied to radiative transfer calculations.

To enable comparison with observational results, we create a dendrogram (Rosolowsky et al. 2008) of the N_H map using AS-TRODENDRO,[2] with a threshold of 10^{22} cm^{-2}, a minimum branching significance of 5×10^{21} cm^{-2}, and a minimum pixel number of 9. We identify dendrogram leaves as 'cores'; column densities are then calculated by averaging all pixels within 0.1 pc of the peak N_H pixel for each leaf, approximating the effects of beam size for single-dish observations of nearby (~ 100 pc) clouds. We compare the results to values inferred from observational data in Fig. 3.
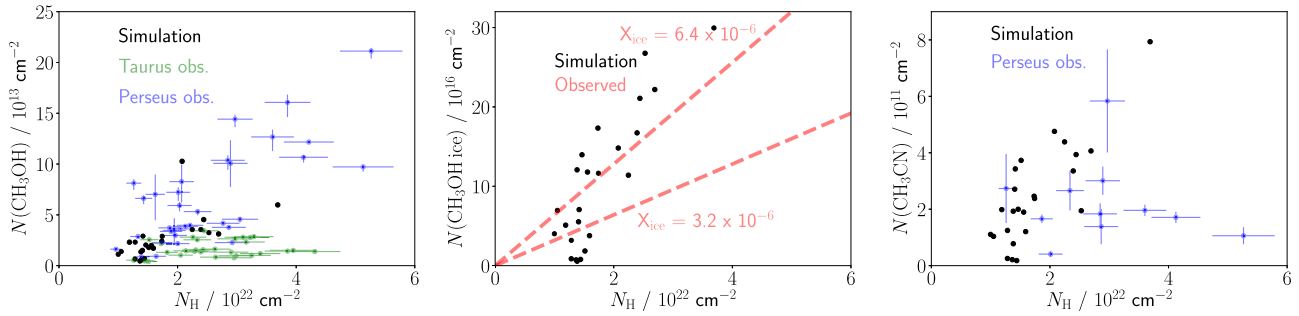
[2]http://www.dendrograms.org/

Figure 3. Left: gas-phase CH₃OH versus total column density for cores from the simulation (black circles), and observed cores in Taurus (green circles; Scibelli & Shirley 2020) and Perseus (blue circles; Scibelli et al. 2024). Centre: ice-phase CH₃OH versus total column density for simulated cores (black circles). The red dashed lines show the observed range of ice-phase methanol abundances in molecular clouds derived from background stars (Boogert, Gerakines & Whittet 2015). Right: gas-phase CH₃CN versus total column density for cores from the simulation (black circles), and observed cores in Perseus (blue circles; Scibelli et al. 2024).
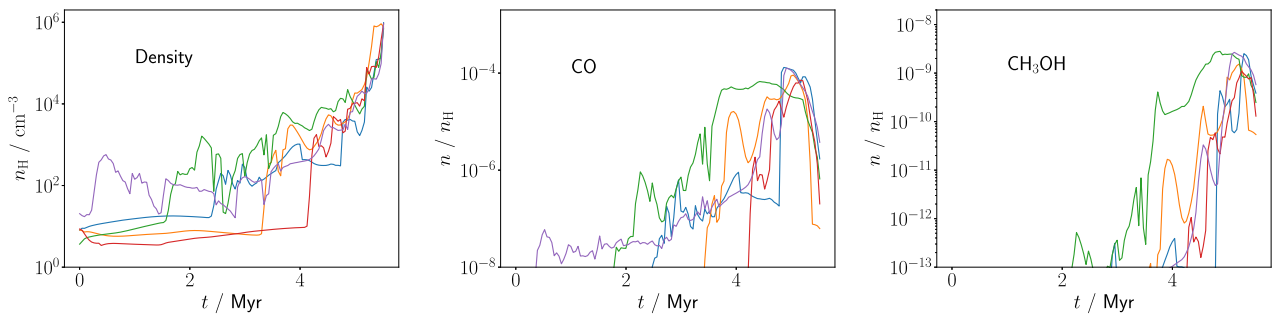
Figure 4. Time evolution of the gas density (left), CO (centre), and CH₃OH (right) abundances for five representative tracer particles (coloured lines), all with final densities of $\sim 10^6 \, \mathrm{cm}^{-3}$.

The simulated cores have comparable gas-phase CH₃OH column densities to observed starless and prestellar cores in the Taurus (Scibelli & Shirley 2020) and Perseus (Scibelli et al. 2024) molecular clouds, which suggests that our methanol formation efficiency of $f_{CH_3OH} = 0.1$ is correctly reproducing the typical gas-phase CH₃OH abundances in real cores. Ice-phase CH₃OH abundances are also comparable to those observed towards background sources along quiescent sightlines (Boogert et al. 2015), and gas-phase CH₃CN column densities are in good agreement with those of Perseus cores for which this molecule is detected (Scibelli et al. 2024). Our simulated cores appear to be similar to real objects in terms of their COM content, which suggests that their COM formation histories may also be similar; this is our working assumption for the remainder of the paper, subject to caveats regarding the limitations of our chemical model discussed in Section 4.1.

The time evolution of the gas density and the CO and CH₃OH abundances for five tracer particles, randomly selected from those with final densities above $6 \times 10^5 \, \mathrm{cm}^{-3}$, are shown in Fig. 4. Despite having similar final densities of $\sim 10^6 \, \mathrm{cm}^{-3}$, the tracers show very different evolutionary histories, with multiple episodes of compression and rarefaction preceding a more-or-less monotonic increase in density to the final value. The diversity in physical evolution results in similarly diverse chemical evolution, with tracers forming (and occasionally losing) significant gas-phase abundances of CO and CH₃OH at different times. However, we note that the late-time monotonic increase in density results in a rapid decline in the gas-phase CO abundance for all tracers due to freeze-out, and that the production of substantial quantities of gas-phase CH₃OH has already occurred prior to this onset of severe CO depletion.

While the time evolution of the tracer abundances appears quite disparate, the evolution with density,[3] shown in Fig. 5, is much more uniform. The CO abundance begins to sharply increase as the gas density approaches $10^3 \, \mathrm{cm}^{-3}$, and reaches a peak value of $\sim 10^{-4}$ at a density of around $10^4 \, \mathrm{cm}^{-3}$. This is mirrored by the gas-phase abundance of CH₃OH, which also begins rising sharply at a density of $10^3 \, \mathrm{cm}^{-3}$, and has essentially reached its peak value by $10^4 \, \mathrm{cm}^{-3}$ for all five tracers. The abundance of CH₃OH ice rises even more sharply with density; the trajectories in density-abundance space are close to vertical at a density of around $3 \times 10^3 \, \mathrm{cm}^{-3}$.

The rapid increase in molecular abundances once a certain density threshold has been reached allows us to define a 'formation density' for each species, characterizing the point at which significant quantities of the molecule (relative to its peak abundance) begin to appear. We identify this as the density at which the abundance of a species first crosses a threshold chosen to be around 10 per cent of the maximum in Fig. 2, although due to the steepness of the trajectories in Fig. 5, our conclusions are relatively insensitive to the exact value chosen; increasing the CH₃OH threshold by an order of magnitude only results in a factor of two difference in the typical formation densities. Fig. 6 shows the distribution of tracers by final density at 5.53 Myr versus the formation density of gas- and ice-phase CH₃OH and gas-phase CH₃CN, with abundance thresholds of 10^{-10}, 10^{-6}, and 10^{-12}, respectively. All three species form at densities below

---

[3]Note that this is the evolution of abundance with density for individual tracer particles over the course of the simulation, as opposed to the distribution of abundance versus density at 5.53 Myr for all tracers in Fig. 2.
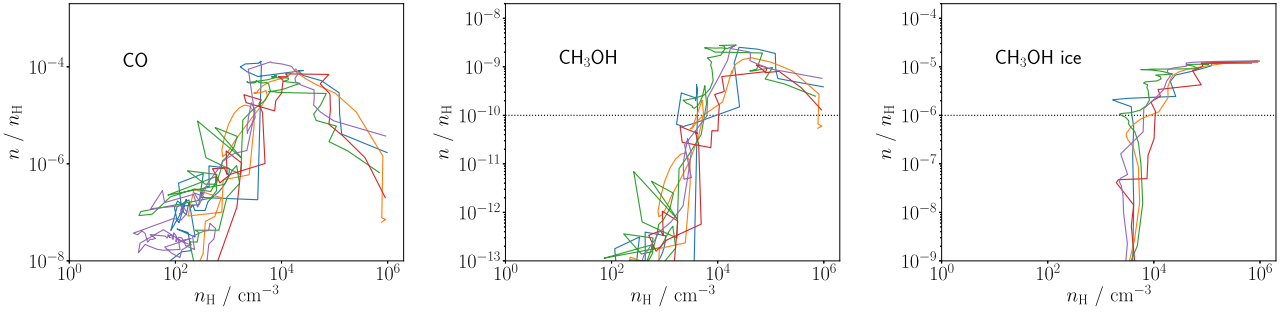
Figure 5. Evolution of gas-phase CO (left), gas-phase CH_3OH (centre), and ice-phase CH_3OH (right) abundances with gas density for the same five tracer particles as in Fig. 4 (coloured lines). Dashed horizontal lines show the threshold abundances used for defining the formation densities in Fig. 6.
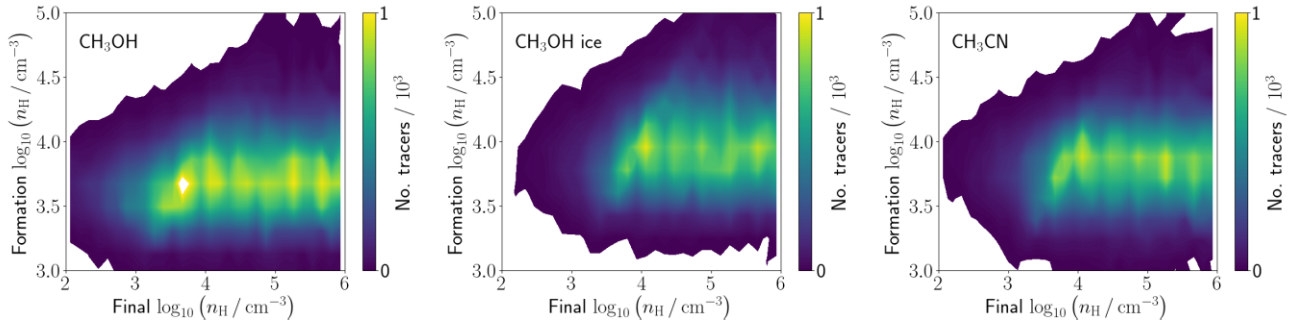

Figure 6. Distribution of tracer particles by final density and formation density of gas-phase CH_3OH (left), ice-phase CH_3OH (centre), and gas-phase CH_3CN (right), for threshold abundances of 10^{-10} for gas-phase CH_3OH, 10^{-6} for ice-phase CH_3OH, and 10^{-12} for gas-phase CH_3CN.

$10^4 \, cm^{-3}$, with significant quantities of gas-phase CH_3OH being produced at densities of only a few $10^3 \, cm^{-3}$. The formation density is effectively constant with regard to the final density of the tracers: material which ends up incorporated into dense cores forms its COM content at the same early evolutionary phase as the surrounding diffuse cloud material.

The methanol formation efficiency of $f_{CH_3OH} = 0.1$ used above results in good agreement with its observed gas- and ice-phase abundances (Fig. 3), but we show in Fig. 7 that our conclusions regarding the formation of COMs are not affected by the exact choice of this parameter. Reducing the formation efficiency by a factor of five results, unsurprisingly, in a lower CH_3OH abundance at all densities, and gas-phase column densities which are now in some tension with the observed values. However, we still find formation densities below $10^4 \, cm^{-3}$, even for an unchanged abundance threshold of 10^{-10} which is close to the maximum value reached. Reducing the threshold to account for the lower peak abundance leads to almost indistinguishable results from those in Fig. 6.

4 DISCUSSION

4.1 Limitations of the chemical model

In addition to the efficiency parameter f_{CH_3OH}, our treatment of CH_3OH formation on grain surfaces relies on the assumptions that hydrogenation is instantaneous (for some fraction of adsorbed CO molecules), that f_{CH_3OH} has a fixed value, and that no further grain surface processes affect the CH_3OH ice after formation. The first of these assumptions is reasonable: simulations which explicitly follow hydrogenation of CO in ice mantles (e.g. Garrod et al.

2022; Molpeceres, Furuya & Aikawa 2024) find that the delay between adsorption of CO and formation of CH_3OH ice is a few kyr, effectively instantaneous in the context of our simulations with a chemical time-step of 44 kyr. The assumption of a fixed f_{CH_3OH} may not hold in all environments, as adsorbed CO may preferentially be converted into CO_2 rather than CH_3OH in unshielded environments with dust temperatures $\gtrsim 12 \, K$ (Garrod & Pauly 2011). Typical grain temperatures in our simulation are $\sim 11 \, K$ for a density of $3000 \, cm^{-3}$ (around the onset of CH_3OH formation) and $10 \, K$ at $10^4 \, cm^{-3}$, so this effect would at most push the formation density of CH_3OH up to the latter value, leaving our conclusions largely unchanged. Finally, additional processes not considered here, such as hydrogen abstraction reactions and photodissociation of mantle species, could reduce the abundance of CH_3OH in the ice and, subsequently, gas phases. As these processes only operate on pre-existing CH_3OH ice, our conclusions regarding the onset of its formation would again be unaffected by their inclusion.

Our treatment of mantle desorption processes, following Roberts et al. (2007), assumes that species are returned to the gas phase with a fixed efficiency per event (H_2 formation or cosmic ray/UV photon impact). The appropriate values for these efficiencies are uncertain, and the approach ignores possible effects such as localized energy deposition (Pantaleone et al. 2021) and desorption of fragments rather than parent species (Bertin et al. 2016), which would tend to reduce the abundance of gas-phase CH_3OH. We again note that this would not change our conclusions regarding early COM formation. Fig. 7 and Fig. A1 demonstrate that the absolute value of a species' abundance has little effect on its formation density, as altering reaction rates leaves the relative behaviour of the abundance with density mostly unchanged. In any case, the formation of CH_3OH
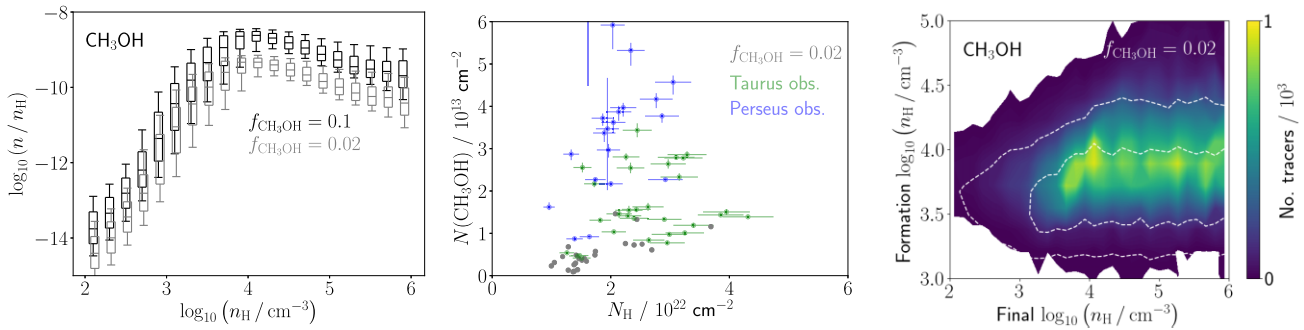
Figure 7. Left: gas-phase CH_3OH abundance versus density for chemical models with $f_{CH_3OH} = 0.1$ (black) and 0.02 (grey). Boxes show median values and 25th/75th percentiles, whiskers the 10th/90th percentiles. Centre: gas-phase CH_3OH versus total column density for cores from the simulation with $f_{CH_3OH} = 0.02$ (grey circles), and observed cores in Taurus (green circles; Scibelli & Shirley 2020) and Perseus (blue circles; Scibelli et al. 2024). Right: distribution of tracer particles by final density and formation density of gas-phase CH_3OH with $f_{CH_3OH} = 0.02$, for a threshold abundance of 10^{-10}. Dashed white lines show the 100- and 500-tracer contours from Fig. 6.

ice would be almost entirely unaffected by changes to desorption processes, given the extremely low gas/ice abundance ratio of this molecule, while desorption has a negligible effect on the gas-phase CH_3CN abundance except at the very highest densities, well beyond the density of its formation via gas-phase reactions.

Our conclusions are robust with respect to changes in the chemical model because the early formation of COMs is primarily a physical effect: in realistic simulations of turbulent molecular clouds, material spends significant periods of time at moderate densities (Fig. 4) before becoming gravitationally bound. This allows the freeze-out of around 10 per cent of the total elemental carbon budget in the form of CO ice at gas densities of a few 10^3 cm^{-3} (Fig. 2). Any chemical model which forms CH_3OH via hydrogenation of CO ice will therefore reach the same conclusions regarding the early formation of this molecule. The prolonged evolution at moderate densities also allows species with gas-phase formation pathways, such as CH_3CN, to exist in quantities which would not be anticipated by studies relying on simplified physical models. Garrod et al. (2022) have also argued for early formation of COMs, but in their case this is due to the inclusion of UV-induced photochemical reactions in ice mantles. Their physical model is a free-fall collapse from an initial density of 3000 cm^{-3}, with pristine atomic chemical initial conditions; we argue instead that by the time material reaches this density, it should already have formed a significant fraction of its final COM content.

4.2 Implications

While there is significant ambiguity in defining what counts as a 'core' and in distinguishing between 'prestellar' and 'starless' objects, both observationally and in simulations (e.g. Offner et al. 2022; Scibelli et al. 2023), a volume density threshold of around 10^4 cm^{-3} is a reasonable choice for separating core material from the ambient cloud (Bergin & Tafalla 2007). Lada, Lombardi & Alves (2010) argue that gas above this density is directly associated with star formation activity, whereas lower density material is not. Similarly, we find in our simulations that material crossing this density threshold almost never returns to lower densities (Priestley et al. 2023b), which can be seen in the nearly monotonic increase in tracer densities in Fig. 4 once a value of 10^4 cm^{-3} has been reached. Under this definition, cores have formed virtually all their COM content before they actually become cores, with COM formation starting at densities of a few 10^3 cm^{-3} and being essentially complete by the time the gas reaches a few 10^4 cm^{-3}.

This stands in stark contrast to the typical approach when modelling COM chemistry in cores (e.g. Vasyunin et al. 2017; Riedel et al. 2023), where the initial abundances are atomic or diffuse-molecular even up to densities of 10^7 cm^{-3}. Slavicinska et al. (2024) recently found that the CH_3OH observed in protostellar cores must have formed in H_2O-rich rather than CO-rich ice, contradicting its assumed origin in heavily CO-depleted cores, but entirely consistent with our proposed formation in lower density cloud material, where most CO is still in the gas phase. We suggest that future work on the chemistry of COMs in cores should account for the fact that these molecules likely already exist in significant quantities before the core itself forms as a distinct object. Moreover, the fact that evolved protostellar systems are observed to continually accrete chemically 'fresh' material from larger scales via streamers (Pineda et al. 2020; Valdivia-Mena et al. 2022, 2023, 2024) makes the composition of this material, and its possible COM content, relevant to studies of disc chemistry and planet formation.

5 CONCLUSIONS

We have simulated the formation of a molecular cloud, and the cores and stars that it contains, from the diffuse ISM, and followed the chemical evolution of the material from atomic initial conditions up to the formation of COMs using a time-dependent gas-grain reaction network. Our approach successfully reproduces the observed abundances of CH_3OH and CH_3CN in starless and prestellar cores. We find that the onset of COM formation occurs at relatively low densities of a few 10^3 cm^{-3}, for both gas- and ice-phase formation pathways.

Although our chemical model is somewhat simplified, particularly in its treatment of grain surface chemistry, this early COM formation is essentially a direct result of the dynamical evolution of the gas, which can spend a considerable amount of time at these moderate densities before undergoing runaway gravitational collapse. It therefore seems likely to be replicated in more sophisticated chemical models, although further studies are required to confirm whether this is in fact the case.

If COMs do form at the low densities that we find here, cores will already be enriched in COMs from the moment they begin to appear as identifiable objects, and complex organic chemistry would originate early, on the scale of molecular clouds, rather than in the later pre- and protostellar evolutionary phases. Astrochemical models would need to account for this prior chemical enrichment to fully understand the delivery of COMs to forming planetary systems.

DATA AVAILABILITY

The data underlying this article will be shared on request.

REFERENCES

Ambrose H. E., Shirley Y. L., Scibelli S., 2021, MNRAS, 501, 347
Bate M. R., Bonnell I. A., Price N. M., 1995, MNRAS, 277, 362
Bergin E. A., Tafalla M., 2007, ARA&A, 45, 339
Bertin M. et al., 2016, ApJ, 817, L12
Boogert A. C. A., Gerakines P. A., Whittet D. C. B., 2015, ARA&A, 53, 541
Booth A. S., Walsh C., Terwisscha van Scheltinga J., van Dishoeck E. F., Ilee J. D., Hogerheijde M. R., Kama M., Nomura H., 2021, Nat. Astron., 5, 684
Ceccarelli C. et al., 2017, ApJ, 850, 176
Clark P. C., Glover S. C. O., Klessen R. S., 2012a, MNRAS, 420, 745
Clark P. C., Glover S. C. O., Klessen R. S., Bonnell I. A., 2012b, MNRAS, 424, 2599
Clément A. et al., 2023, A&A, 675, A165
Garrod R. T., Herbst E., 2006, A&A, 457, 927
Garrod R. T., Jin M., Matis K. A., Jones D., Willis E. R., Herbst E., 2022, ApJS, 259, 1
Garrod R. T., Pauly T., 2011, ApJ, 735, 15
Genel S., Vogelsberger M., Nelson D., Sijacki D., Springel V., Hernquist L., 2013, MNRAS, 435, 1426
Giani L., Ceccarelli C., Mancini L., Bianchi E., Pirani F., Rosi M., Balucani N., 2023, MNRAS, 526, 4535
Glover S. C. O., Clark P. C., 2012, MNRAS, 421, 116
Glover S. C. O., Mac Low M.-M., 2007, ApJS, 169, 239
Gong M., Ostriker E. C., Wolfire M. G., 2017, ApJ, 843, 38
Habing H. J., 1968, Bull. Astron. Inst. Netherlands, 19, 421
Herbst E., van Dishoeck E. F., 2009, ARA&A, 47, 427
Holdship J., Viti S., 2022, A&A, 658, A103
Holdship J., Viti S., Jiménez-Serra I., Makrymallis A., Priestley F., 2017, AJ, 154, 38
Hunter G. H., Clark P. C., Glover S. C. O., Klessen R. S., 2023, MNRAS, 519, 4152
Indriolo N. et al., 2015, ApJ, 800, 40
Jenkins E. B., 2009, ApJ, 700, 1299
Jensen S. S., Jørgensen J. K., Furuya K., Haugbølle T., Aikawa Y., 2021a, A&A, 649, A66
Jensen S. S., Jørgensen J. K., Kristensen L. E., Coutens A., van Dishoeck E. F., Furuya K., Harsono D., Persson M. V., 2021b, A&A, 650, A172
Jensen S. S., Spezzano S., Caselli P., Grassi T., Haugbølle T., 2023, A&A, 675, A34
Jiménez-Serra I. et al., 2016, ApJ, 830, L6
Jiménez-Serra I. et al., 2020, Astrobiology, 20, 1048
Jiménez-Serra I., Vasyunin A. I., Spezzano S., Caselli P., Cosentino G., Viti S., 2021, ApJ, 917, 44
Jin M., Garrod R. T., 2020, ApJS, 249, 26
Jørgensen J. K. et al., 2016, A&A, 595, A117
Lada C. J., Lombardi M., Alves J. F., 2010, ApJ, 724, 687
Liszt H., Gerin M., Beasley A., Pety J., 2018, ApJ, 856, 151
McClure M. K. et al., 2023, Nat. Astron., 7, 431
McElroy D., Walsh C., Markwick A. J., Cordiner M. A., Smith K., Millar T. J., 2013, A&A, 550, A36
Megías A., Jiménez-Serra I., Martín-Pintado J., Vasyunin A. I., Spezzano S., Caselli P., Cosentino G., Viti S., 2023, MNRAS, 519, 1601
Mininni C. et al., 2021, A&A, 653, A87
Molpeceres G., Furuya K., Aikawa Y., 2024, A&A, 688, A150
Nazari P. et al., 2024, A&A, 686, A71
Öberg K. I., Bergin E. A., 2021, Phys. Rep., 893, 1
Offner S. S. R. et al., 2022, MNRAS, 517, 885
Pakmor R., Bauer A., Springel V., 2011, MNRAS, 418, 1392
Pantaleone S., Enrique-Romero J., Ceccarelli C., Ferrero S., Balucani N., Rimola A., Ugliengo P., 2021, ApJ, 917, 49
Pineda J. E., Segura-Cox D., Caselli P., Cunningham N., Zhao B., Schmiedeke A., Maureira M. J., Neri R., 2020, Nat. Astron., 4, 1158
Priestley F. D., Clark P. C., Glover S. C. O., Ragan S. E., Fehér O., Prole L. R., Klessen R. S., 2023a, MNRAS, 524, 5971
Priestley F. D., Clark P. C., Glover S. C. O., Ragan S. E., Fehér O., Prole L. R., Klessen R. S., 2023b, MNRAS, 526, 4952
Punanova A., Vasyunin A., Caselli P., Howard A., Spezzano S., Shirley Y., Scibelli S., Harju J., 2022, ApJ, 927, 213
Rawlings J. M. C., Hartquist T. W., Menten K. M., Williams D. A., 1992, MNRAS, 255, 471
Rawlings J. M. C., Keto E., Caselli P., 2024, MNRAS, 530, 3986
Riedel W., Sipilä O., Redaelli E., Caselli P., Vasyunin A. I., Dulieu F., Watanabe N., 2023, A&A, 680, A87
Roberts J. F., Rawlings J. M. C., Viti S., Williams D. A., 2007, MNRAS, 382, 733
Rocha W. R. M. et al., 2024, A&A, 683, A124
Rosolowsky E. W., Pineda J. E., Kauffmann J., Goodman A. A., 2008, ApJ, 679, 1338
Sabatini G., Bovino S., Redaelli E., 2023, ApJ, 947, L18
Scibelli S., Shirley Y., 2020, ApJ, 891, 73
Scibelli S., Shirley Y., Megías A., Jiménez-Serra I., 2024, MNRAS, 533, 4104
Scibelli S., Shirley Y., Schmiedeke A., Svoboda B., Singh A., Lilly J., Caselli P., 2023, MNRAS, 521, 4579
Scibelli S., Shirley Y., Vasyunin A., Launhardt R., 2021, MNRAS, 504, 5754
Sembach K. R., Howk J. C., Ryans R. S. I., Keenan F. P., 2000, ApJ, 528, 310
Slavicinska K. et al., 2024, A&A, 688, A29
Spezzano S. et al., 2022, A&A, 657, A10
Springel V., 2010, MNRAS, 401, 791
Tress R. G., Smith R. J., Sormani M. C., Glover S. C. O., Klessen R. S., Mac Low M.-M., Clark P. C., 2020, MNRAS, 492, 2973
Valdivia-Mena M. T. et al., 2022, A&A, 667, A12
Valdivia-Mena M. T. et al., 2023, A&A, 677, A92

Valdivia-Mena M. T. et al., 2024, A&A, 687, A71
Vasyunin A. I., Caselli P., Dulieu F., Jiménez-Serra I., 2017, ApJ, 842, 33
Viti S., Collings M. P., Dever J. W., McCoustra M. R. S., Williams D. A., 2004, MNRAS, 354, 1141
Walsh C. et al., 2016, ApJ, 823, L10
Yin C., Priestley F. D., Wurster J., 2021, MNRAS, 504, 2381

APPENDIX A: THE CH₃CN FORMATION RATE

Giani et al. (2023) have recently reevaluated the formation pathways of CH_3CN, recommending a significantly lower rate for the dissociative recombination reaction between CH_3CNH^+ and free electrons compared to the UMIST12 value (normalization at 300 K of 2.2×10^{-8} cm³ s^{-1} versus 5.3×10^{-7} cm³ s^{-1}, in addition to a steeper temperature dependence). We have chosen to adopt their rate coefficients for this reaction, which produces good agreement with observed CH_3CN column densities (Fig. 3), but as with the methanol

formation efficiency parameter, our main conclusions still hold when using the original UMIST12 values.

Fig. A1 shows that the UMIST12 rate coefficients result in roughly an order of magnitude increase in gas-phase CH_3CN abundance at fixed density compared to the Giani et al. (2023) values, which leads to a significant tension between predicted and observed column densities for this molecule. However, the qualitative relationship between the abundance and gas density is largely unaffected. We therefore find that the CH_3CN formation density, defined using an increased threshold abundance of 10^{-11} to reflect the higher peak values, is effectively indistinguishable from the results in Fig. 6. Fig. A1 and Fig. 7 demonstrate that while the absolute quantity of COMs formed depends on the details of the chemical model, the onset of COM formation does not, occurring at volume densities consistently below those associated with cores.
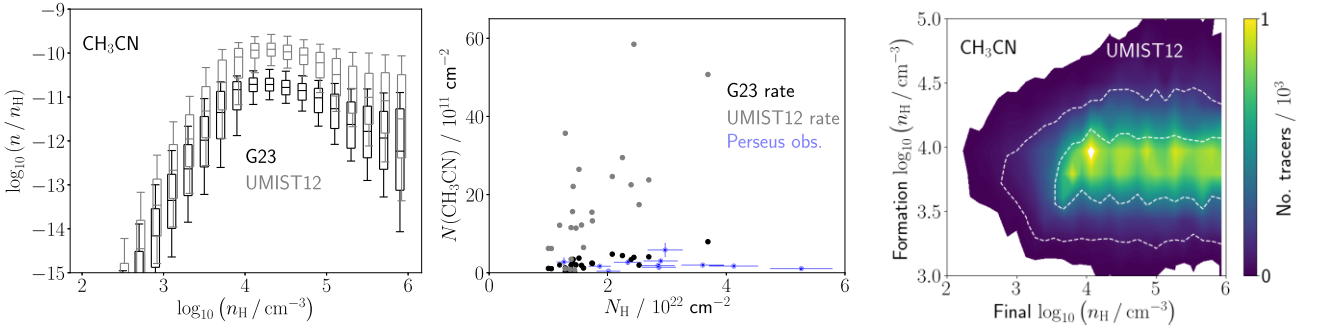

Figure A1. Left: gas-phase CH_3CN abundance versus density for chemical models with the Giani et al. (2023, black) and UMIST12 (grey) rates for dissociative recombination of CH_3CNH^+. Boxes show median values and 25th/75th percentiles, whiskers the 10th/90th percentiles. Centre: gas-phase CH_3CN versus total column density for cores from the simulation using the Giani et al. (2023, black circles) and UMIST12 (grey circles) rates, and observed cores in Perseus (blue circles; Scibelli et al. 2024). Right: distribution of tracer particles by final density and formation density of gas-phase CH_3CN using the UMIST12 rate, for a threshold abundance of 10^{-11}. Dashed white lines show the 100- and 500-tracer contours from Fig. 6.

This paper has been typeset from a TeX/LaTeX file prepared by the author.